

Two-Zone Elastic-Plastic Single Shock Waves in Solids

Vasily V. Zhakhovsky,¹ Mikalai M. Budzevich,¹ Nail A. Inogamov,² Ivan I. Oleynik,^{1,*} and Carter T. White³

¹*Department of Physics, University of South Florida, Tampa, Florida 33620, USA*

²*Landau Institute for Theoretical Physics, RAS, Chernogolovka 142432, Russia*

³*Naval Research Laboratory, Washington, D.C. 20375, USA*

(Received 22 June 2011; published 22 September 2011)

By decoupling time and length scales in moving window molecular dynamics shock-wave simulations, a new regime of shock-wave propagation is uncovered characterized by a two-zone elastic-plastic shock-wave structure consisting of a leading elastic front followed by a plastic front, both moving with the same average speed and having a fixed net thickness that can extend to microns. The material in the elastic zone is in a metastable state that supports a pressure that can substantially exceed the critical pressure characteristic of the onset of the well-known split-elastic-plastic, two-wave propagation. The two-zone elastic-plastic wave is a general phenomenon observed in simulations of a broad class of crystalline materials and is within the reach of current experimental techniques.

DOI: [10.1103/PhysRevLett.107.135502](https://doi.org/10.1103/PhysRevLett.107.135502)

PACS numbers: 62.50.Ef, 02.70.Ns, 62.20.D-, 62.20.F-

Shock waves propagate through solids at supersonic speeds and, if powerful enough, can induce irreversible plastic deformations [1–4]. Although this shock-induced plasticity has been the focus of intense experimental [5,6] and theoretical [7–11] investigations, the atomic scale mechanisms coupling the high-strain-rate plastic deformations to the initial elastic compression remain poorly understood. Herein, we report the observation of a new regime of shock-wave propagation that should be considered in any study of shock-induced plasticity in solids. This regime, illustrated for Al but also observed by us in simulations of a wide range of other materials, is characterized by a two-zone elastic-plastic shock-wave structure consisting of a leading elastic zone followed by a plastic zone, both moving at the same speed. The elastic front is overdriven by the plastic front but—in contrast to the usual picture—is not overrun. Rather, the elastic zone behind this front can extend to an appreciable fraction of a micron or more.

The observation of a single two-zone elastic-plastic wave, with high elastic pressures and large elastic zone lengths, was made possible by a moving window (MW) simulation method that decouples time and length scales in molecular dynamics (MD) shock-wave simulations [12]. Most previous shock simulations were done using a piston-driven setup that couples time and length scales because the number of atoms that have to be treated explicitly grows with time as the shock wave separates from the piston face. The MW-MD method avoids this stumbling block by simulating the material in a reference frame of the shock-wave front. Like standard piston-driven simulations, the MW method assumes a simulation cell with periodic boundary conditions imposed in directions lateral to the direction of shock front propagation. Unlike piston simulations, however, crystalline material is fed into a MW simulation upstream from the shock wave and removed self-consistently downstream [13], thus allowing the

complex processes taking place behind the shock-wave front to be simulated over an indefinite period of time.

To describe the major features of the two-zone elastic-plastic regime, consider the particular case of a relatively strong shock wave propagating in the [111] direction in a perfect Al crystal supported by a steadily moving piston with velocity $u_p = 2284$ m/s. Figure 1 shows a snapshot of the internal shock-wave structure consisting of an elastic zone of length 94 nm followed by a plastic zone of length ≈ 120 nm, both moving with the same speed $u_s = 8562$ m/s. The distinction between the elastic and plastic zones (green/red and black colors, respectively) is easily seen in the 2D maps of both shear stress $\tau(x, y)$ and the local-atomic-order parameter Q_4 [14], with the latter also used to visualize clearly the appearance of dislocations at the end of the elastic zone.

The elastic zone has a rich internal structure due to the propagation of localized ultrashort elastic pulses emitted by dislocations generated within the plastic shock front. See video in the Supplemental Material. These triangle-shaped pulses propagate toward the leading elastic front with the local sound speed in the nonuniformly compressed elastic zone. Later, they combine into a series of planar elastic shock pulses that decrease in amplitude and speed as they approach the leading elastic front. These elastic pulses synchronize the speeds of the elastic and plastic fronts resulting in a constant average elastic zone length.

The plastic shock front also exhibits rich local dynamics due to the homogeneous nucleation of dislocation loops and their avalanche multiplication. See Fig. 1. The shear stress drops substantially between 66–75 nm accompanied by a fast increase of dislocation loop concentration. Thereafter, it slowly decreases towards a small equilibrium value at the end of the plastic zone. As a result of such complicated dislocation dynamics, the overall thickness of the plastic zone can be appreciable, reaching hundreds of

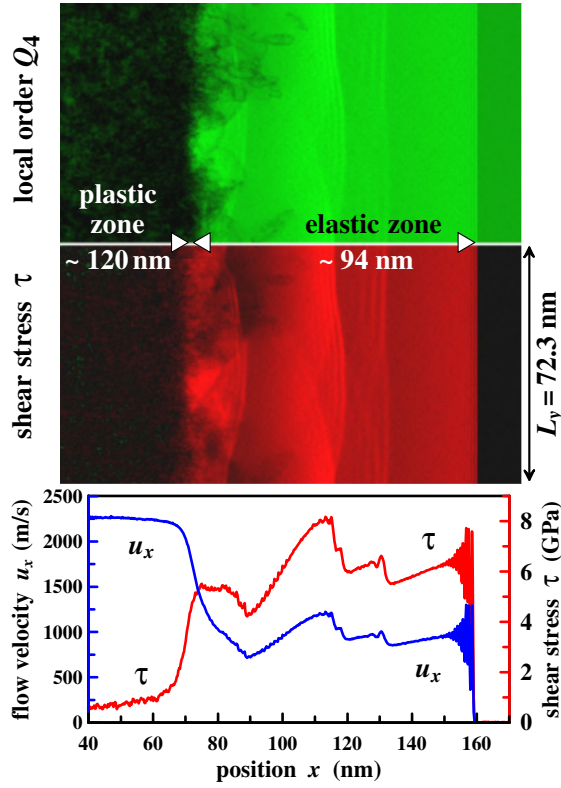


FIG. 1 (color online). Internal structure of a two-zone elastic-plastic single shock wave propagating along the [111] direction in a perfect Al crystal with shock speed 8562 m/s (corresponding piston velocity 2284 m/s). Top and middle panels: 2D maps of local order parameter Q_4 and shear stress, respectively. Bottom panel: mass velocity and shear stress profiles. The MW simulation cell used to obtain these results contains $35.32 \pm 0.01 \times 10^6$ atoms within a box with dimensions $L_x = 400$ nm, $L_y = 72.3$ nm, and $L_z = 15.9$ nm. The pressure and temperature in the undisturbed sample were $P_0 = 0$ and $T_0 = 300$ K, respectively.

nanometers in a relatively weak two-zone elastic-plastic single shock wave.

To see how this two-zone single shock-wave regime lies outside the traditional picture of shock-induced elastic-plastic transitions [2–4], consider the shock Hugoniot—the locus of allowed final shock states with longitudinal pressure P_{xx} and the volume V for a material initially in the state O of Fig. 2. At shock-wave intensities below the Hugoniot elastic limit (HEL), $P_{xx} < P_{HEL}$, only a single elastic shock wave propagates through the crystal with the material transforming from the initial to the final state along a cord, known as the Rayleigh line, connecting these states lying on the Hugoniot. As P_{xx} exceeds the threshold pressure P_{HEL} , however, the material’s response changes due to plastic deformations causing this single front to split into a fast elastic precursor and a slow plastic wave. Now consider the point SP on the Hugoniot in this split shock-wave regime. Then, in the reference frame of the material behind the elastic front, the ratio of the speed of the leading

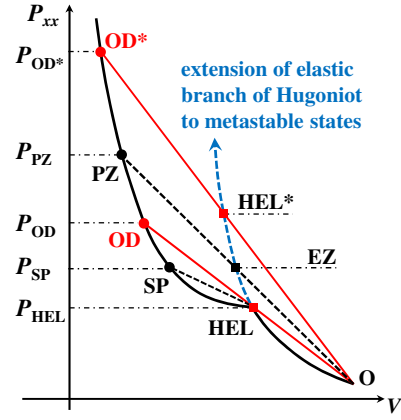


FIG. 2 (color online). Schematic of P - V shock Hugoniot, consisting of elastic and plastic branches intersecting at the HEL. For a shock compression within the interval $P_{OD} < P_{PZ} < P_{OD}^*$ the Rayleigh line PZ intersects an extension of the elastic branch of the Hugoniot (blue dashed line) at point EZ, leading to a two-zone elastic-plastic shock wave for which the states within the elastic and plastic zones are indicated by points EZ and PZ, respectively.

elastic front to the following plastic front is given by $R = \sqrt{S_O^{HEL}/S_{HEL}^{SP}}$, where S_O^{HEL} and S_{HEL}^{SP} denote the slopes of the Rayleigh lines from O to HEL and from HEL to SP, respectively [1]. Because the speed of the elastic precursor is determined only by the properties of O and the cusp at HEL, it remains unchanged with further increase in P_{xx} , even as the slower plastic front increases in speed. Eventually, at the onset of the overdriven regime $P_{xx} = P_{OD}$, whereupon $R = 1$ and the velocities of the elastic precursor and the plastic fronts become equal.

It is often thought that at shock-wave intensities $P_{xx} > P_{OD}$, the elastic precursor is effectively overrun leaving only a single plastic front. However, such an interpretation is wrong. In fact, the two-zone elastic-plastic regime found in our simulations corresponds to shock intensities $P_{xx} > P_{OD}$. This two-zone elastic-plastic regime is characterized by a finite and potentially large separation between the elastic and plastic fronts, both moving with the same average speed.

For a specific shock intensity, $P_{PZ} > P_{OD}$, the state of the crystal in the elastic zone is represented in Fig. 2 by the point EZ that lies at the intersection of the Rayleigh line (O-PZ) with the extension of the elastic branch of the Hugoniot beyond the HEL. This metastable elastic state EZ decays into the plastic state PZ during the development of plastic deformations via dislocation loop nucleation and multiplication in the plastic zone. The corresponding time scale for the elastic-plastic transition is long enough to produce a *finite* elastic zone ahead of the plastic shock front of appreciable thickness. The upper limit P_{OD}^* for this two-zone regime corresponds to an effective disappearance of the elastic zone. Therefore, it is for final state pressures such that $P_{OD} < P_{xx} < P_{OD}^*$ that the two-zone

regime does not fit into the traditional picture of shock-induced elastic-plastic transitions.

All four regimes of shock-wave propagation outlined above were systematically investigated for an Al crystal shocked along the [111] crystallographic direction using both MW and standard piston MD simulations; the piston simulations were necessary to treat the split shock-wave regime, where the elastic and plastic fronts move at different speeds. The gray sector in Fig. 3 covers the interval of applied pressures $51 \text{ GPa} < P_{xx} < 65 \text{ GPa}$ corresponding to the newly uncovered two-zone elastic-plastic single shock-wave regime. The calculated P - V Hugoniot is in good agreement with available experimental data [15–17], which demonstrates the excellent quality of the new embedded atom potential for Al used in our simulations [18]. However, the HEL for the perfect Al crystal obtained from the MD simulations, $P_{\text{HEL}} = 21.3 \text{ GPa}$, is too high compared to experiment, as shown by the two recent experimental points (blue crosses in Fig. 3) corresponding to the observation of a plastic regime of shock propagation in single crystal Al [17]. Such disagreement indicates the importance of preexisting defects in lowering the simulated HEL for the perfect crystal towards experimental values obtained from imperfect samples. Indeed, once vacancies at a concentration of 10^{-3} are introduced into the crystalline sample, an almost twofold reduction of the HEL to $P_{\text{HEL}} = 12.6 \text{ GPa}$ results. A similar level of HEL reduction upon the introduction of defects was also calculated for crystalline copper [19].

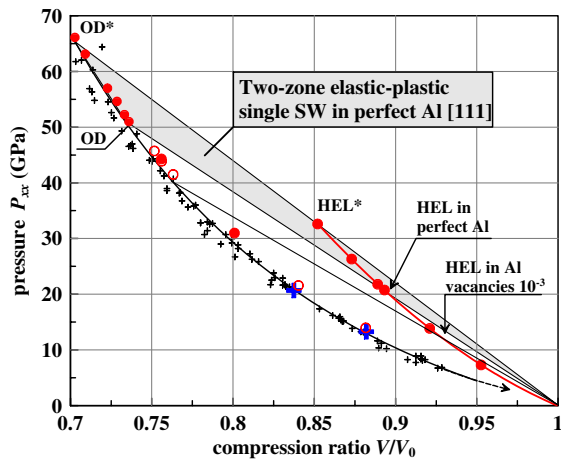


FIG. 3 (color online). P - V Hugoniot for a perfect Al [111] crystal and a sample with a vacancy concentration of 10^{-3} . Solid red circles are from the perfect crystal, red open circles from the crystal with vacancies, crosses from experimental data [15], and the black solid line is a fit of experimental data points [16]. The two blue crosses are from experiments on single crystals [17]. The dashed line terminating in an arrow yields a cusp at around 1 GPa, consistent with the experimental observation of an elastic precursor corresponding to such a HEL for polycrystalline samples that are able to support such weak plastic shock waves.

The fixed average length of the elastic zone d_{el} within the two-zone elastic-plastic regime is appreciable and becomes extremely large when the applied pressure P_{xx} approaches P_{OD} from above. Figure 4 shows calculated values of d_{el} as a function of the average elastic pressure P_{el} read from simulated elastic pressure profiles for applied pressures in the interval $P_{\text{OD}} < P_{xx} < P_{\text{OD}}^*$. The elastic states of material with $P_{\text{el}} > P_{\text{HEL}}$ lie along the extension of the elastic branch of the Hugoniot into the metastable area above the HEL depicted in Figs. 2 and 3. The largest d_{el} ($\approx 400 \text{ nm}$) that we were able to simulate in the perfect Al [111] crystal corresponds to $u_s = 8501 \text{ m/s}$, with a total shock-wave front thickness close to $1 \mu\text{m}$. The sharp increase in d_{el} shown in Fig. 4, as $P_{\text{el}} \rightarrow P_{\text{HEL}}$, corresponding to $P_{xx} \rightarrow P_{\text{OD}}$, indicates that d_{el} might asymptotically approach infinity as the plastic shock intensity approaches this limit from above, provided very slow relaxation processes due to stress and thermal activation of defects in the elastic zone are ignored. Note that very large-scale piston simulations, which must be extended to over 150 ps, can also be used to obtain the 33 nm point of Fig. 4. See the Supplemental Material [13]. However, owing to computational limitations, the MW-MD method was needed to obtain the points of Fig. 4 corresponding to much larger elastic zone lengths.

By assuming that $d_{\text{el}} \propto (P_{\text{el}} - P_{\text{HEL}})^\alpha$ in fitting the MW-MD results near the HEL, a critical pressure $P_{\text{HEL}} = 21.3 \text{ GPa}$ is obtained that is very close to the P_{HEL} calculated independently from piston MD simulations of split shock waves. In the opposite limit of increasing shock-wave intensities, where $P_{\text{el}} \rightarrow P_{\text{HEL}}^*$, corresponding to $P_{xx} \rightarrow P_{\text{OD}}^*$, the elastic zone shrinks from a significant fraction of a micron to several nanometers, and finally effectively disappears at $P_{\text{HEL}}^* \approx 33.5 \text{ GPa}$.

A similar behavior in the elastic zone length as a function of shock intensity is observed for an Al crystal with preexisting vacancies. See Fig. 4. As expected, the

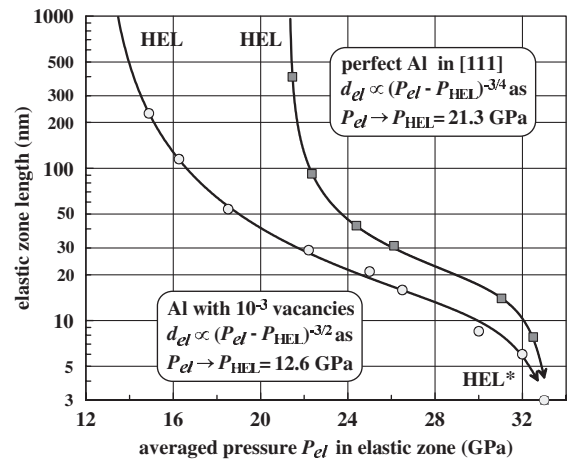


FIG. 4. Elastic zone length as a function of average pressure in the elastic zone for both a perfect Al crystal and a sample containing vacancies with concentration 10^{-3} .

introduction of defects significantly reduces both the length of the elastic zone (from 400 nm to 20 nm for a shock wave propagating with $u_s = 8501$ m/s) and P_{HEL} (from 21.3 GPa to 12.6 GPa). However, the presence of vacancies does not appreciably affect P_{HEL}^* , which corresponds to the effective disappearance of the elastic zone. This is understandable because at such a high pressure the dislocations appear on a much smaller length scale than the average distance between preexisting vacancies.

A large value of elastic pressure is a distinct feature of the two-zone elastic-plastic regime consistent with the observation of the anomalously high elastic wave amplitudes in recent laser-driven experiments [20–22] on Al. In particular, a leading elastic wave 150 nm long supporting a pressure of 12 GPa was detected in experiments by Whitley *et al.* [20]. Although the increasing length of the high-pressure elastic zone with time observed by Whitley *et al.* is consistent with shock-wave splitting, its decreasing amplitude is not, as this amplitude is determined by the HEL that simulations show is effectively independent of the applied pressure in the Al split shock-wave regime. This behavior, however, is consistent with an overdriven elastic wave as the elastic zone will both increase in length and decrease in amplitude with decreasing pressure support from the driving laser pulse. Another indirect sign of the existence of the two-zone elastic-plastic regime is the presence of a small elastic shoulder pinned to the plastic wave observed in previous MD simulations [9,23–25].

Although the physics of the two-zone, elastic-plastic regime was illustrated using Al, this is a general phenomenon that should be observed in a broad class of crystalline materials. Indeed, we have already found such a two-zone, elastic-plastic single wave regime in simulations of Ni, Au, and diamond samples, as well as in Lennard-Jones solids. To provide direct experimental proof of the two-zone regime, however, the time delay between arrivals of the elastic and plastic fronts at the free surface of the sample should be measured with picosecond resolution, and shown to be independent of sample thickness. Such measurements are within the reach of the current laser-driven shock-wave experiments.

The work at USF and NRL was supported by ONR and NRL. The work at USF was also supported by the NSF. N. A. I. was supported by the Russian Fund for Basic Research. Simulations were performed using the NSF TeraGrid facilities, the USF Research Computing Cluster, and the computational facilities of Materials Simulation Laboratory at USF.

*oleynik@usf.edu

[1] Y. B. Zel'dovich and Y. P. Raizer, *Physics of Shock Waves and High-Temperature Hydrodynamic Phenomena* (Dover, New York, 2002).

- [2] *Shock Waves in Condensed Media*, edited by P. Caldirola and H. Knoepfel (Academic Press, New York, 1971).
- [3] R. A. Graham, *Solids Under High-Pressure Shock Compression: Mechanics, Physics, and Chemistry* (Springer, New York, 1993).
- [4] G. I. Kanel, S. V. Razorenov, and V. E. Fortov, *Shock-Wave Phenomena and the Properties of Condensed Matter* (Springer, New York, 2004).
- [5] D. H. Kalantar, J. F. Belak, G. W. Collins, J. D. Colvin, H. M. Davies, J. H. Eggert, T. C. Germann, J. Hawreliak, B. L. Holian, K. Kadau *et al.*, *Phys. Rev. Lett.* **95**, 075502 (2005).
- [6] K. Rosolankova, J. S. Wark, E. M. Bringa, and J. Hawreliak, *J. Phys. Condens. Matter* **18**, 6749 (2006).
- [7] B. L. Holian and P. S. Lomdahl, *Science* **280**, 2085 (1998).
- [8] T. C. Germann, J. E. Hammerberg, and B. L. Holian, *AIP Conf. Proc.* **706**, 285 (2004).
- [9] K. Kadau, T. C. Germann, P. S. Lomdahl, and B. L. Holian, *Phys. Rev. B* **72**, 064120 (2005).
- [10] E. M. Bringa, A. Caro, Y. Wang, M. Victoria, J. M. McNaney, B. A. Remington, R. F. Smith, B. R. Torralva, and H. Swygenhoven, *Science* **309**, 1838 (2005).
- [11] E. M. Bringa, K. Rosolankova, R. E. Rudd, B. A. Remington, J. S. Wark, M. Duchaineau, D. H. Kalantar, J. Hawreliak, and J. Belak, *Nature Mater.* **5**, 805 (2006).
- [12] V. V. Zhakhovskii, K. Nishihara, and S. I. Anisimov, *JETP Lett.* **66**, 99 (1997).
- [13] See Supplemental Material at <http://link.aps.org/supplemental/10.1103/PhysRevLett.107.135502> for more details on the moving window method and its validation.
- [14] P. J. Steinhardt, D. R. Nelson, and M. Ronchetti, *Phys. Rev. B* **28**, 784 (1983).
- [15] Shock wave database: <http://teos.ficp.ac.ru/rusbank/>.
- [16] M. P. Desjarlais (private communication).
- [17] H. Huang and J. R. Asay, *J. Appl. Phys.* **101**, 063550 (2007).
- [18] V. V. Zhakhovskii, N. A. Inogamov, Y. V. Petrov, S. I. Ashitkov, and K. Nishihara, *Appl. Surf. Sci.* **255**, 9592 (2009).
- [19] R. Ravelo, B. L. Holian, and T. C. Germann, *AIP Conf. Proc.* **1195**, 825 (2009).
- [20] V. H. Whitley, S. D. McGrane, D. E. Eakins, C. A. Bolme, D. S. Moore, and J. F. Bingert, *J. Appl. Phys.* **109**, 013505 (2011).
- [21] S. I. Ashitkov, M. B. Agranat, G. I. Kanel', P. S. Komarov, and V. E. Fortov, *JETP Lett.* **92**, 516 (2010).
- [22] M. R. Armstrong, J. C. Crowhurst, S. Bastea, and J. M. Zaig, *J. Appl. Phys.* **108**, 023511 (2010).
- [23] V. V. Zhakhovskii, S. V. Zybin, K. Nishihara, and S. I. Anisimov, *Prog. Theor. Phys. Suppl.* **138**, 223 (2000).
- [24] S. V. Zybin, M. L. Elert, and C. T. White, *Phys. Rev. B* **66**, 220102 (2002).
- [25] E. M. Bringa, J. U. Cazamias, P. Erhart, J. Stölken, N. Tanushev, B. D. Wirth, R. E. Rudd, and M. J. Caturla, *J. Appl. Phys.* **96**, 3793 (2004).